

Coalescence of Polymer Droplets Moving on a Surface with Stiffness Gradient

Divyansh Tripathi^{1,*}, Vimal Kishore^{1,†}, Panagiotis E. Theodorakis², and Swarn Lata Singh^{3‡}

¹ *Department of Physics, Banaras Hindu University, Varanasi 221005, India*

² *Institute of Physics, Polish Academy of Sciences,
Al. Lotników 32/46, 02-668 Warsaw, Poland*

³ *Department of Physics, Mahila Mahavidyalaya,
Banaras Hindu University, Varanasi 221005, India*

(Dated: May 19, 2026)

Abstract

Coalescence of sessile droplets has been in the focus of current and previous research, due to its relevance for various biological processes and industrial applications. However, the coalescence of moving droplets on substrates with varying properties, such as gradient substrates, has received less attention. Hence, the main focus here is on the coalescence of droplets that are moving in the same direction on a soft surface; the motion of the droplets is caused by a gradient in the surface stiffness. As reference, stationary coalescence of the same droplets is also studied on the corresponding uniform surfaces for different stiffness values. To describe the coalescence phenomenon on a surface with stiffness gradient, a relevant range of velocity ratios of the leading and the trailing droplet was considered to elucidate the effect of this parameter on coalescence. Moreover, to analyze the dynamics of the process, the temporal growth of the bridge height (h) was investigated, which follows a power law ($h \sim t^\alpha$), before eventually attaining a constant value. The obtained values of α show a transition from a higher to a lower value as a function of time, pointing to the presence of two distinct power-law growth regimes, where the transition signifies the crossover from the capillarity-dominated regime to the viscoelasticity-dominated regime of coalescence. In addition, varying attractive strengths for droplet–droplet and intra-droplet interactions were considered. The results indicate that both the dynamics and the degree of the coalescence strongly depend on these interaction parameters. Thus, we anticipate that our results will shed more light on the durotaxis-driven coalescence of polymeric droplets for various relevant system parameters, which will have practical implications for applications ranging from microfluidics to ink-jet printing, where substrate properties may vary. In addition, results may add to the fundamental understanding of the interactions among multicellular aggregates moving on biological surfaces.

I. INTRODUCTION

Droplet interactions are of fundamental importance in a wide range of industrial applications. The texture and the stability of emulsions, which make the very basis of various food, cosmetics, and pharmaceutical products, greatly depends on the interaction among constituent droplets [1–3]. Further examples include but are not limited to applications in

* divyanshtripathi@bhu.ac.in

† vimalk@bhu.ac.in

‡ swarn@bhu.ac.in

microfluidics, spray cooling, coating, printing and oil–water separation [4–7]. Interacting droplets have also gained attention as a model system to study the interaction between cells and cellular aggregates [8, 9]. Such studies are also helpful in gaining insights into biological processes such as the interaction of immune cells with pathogens, and the formation of tissue and growth of bacterial colonies [10–15]. In such cases, fundamentally understanding the effect of relevant system parameters that dictate the interplay between the droplets could lead to better droplet control in applications ranging from microfluidics [16], to biomedical [17] and chemical applications [18]. In those, the various parameters influencing the droplet behavior include the fluid properties of the droplets, their mutual interactions, geometries (whether the droplet is sessile, or pendant), their approach velocities, and the presence of external forces [19, 20].

The capillarity driven merging of two or more droplets to form a single droplet is one of the most well studied phenomena in the literature [21–28]. In a rather simple scenario, namely the coalescence of freely suspended, miscible droplets of a Newtonian fluid, the dynamics of the coalescence process can be described through the rate of the radius growth of the liquid bridge, which forms between the coalescing droplets. In particular, it has been shown that the temporal growth of the bridge radius follows a power-law scaling with time. However, the exponent of the scaling is not universal, since it depends on various system parameters. For example, for freely suspended Newtonian droplets, the radius of the bridge grows linearly with time ($\propto t$) in the viscous regime, where the resistance to coalescence is predominantly attributed to viscous forces, while the role of the inertia can be neglected [29, 30]. In contrast, in the inertia dominated regime, the bridge radius growth is proportional to $t^{0.5}$ [21, 31]. A third regime has also been reported in the literature, namely the inertially limited viscous (ILV) regime, which occurs when both viscosity and inertia are comparable. Some studies have reported ILV as the initial regime for all coalescence events [32]. A transition from the ILV behavior to either the viscous or the inertial regimes depends on the fluid properties of the droplet and its size [32–36].

Only a few studies have thus far concerned interacting, non-Newtonian droplets in the literature. In this case, various factors are supposed to affect the dynamics of coalescence, such as the elastic properties of the droplets and the intrinsic time scale for relaxation [33]. Here, examples of non-Newtonian fluids range from polymeric solutions to liquid-crystal and biological soft matter, where structural properties at microscopic level substantially vary for

each sub-class. As a result, a unique response is expected for each of these materials, which renders difficult the formulation of a unified framework that could describe the coalescence in the case of non-Newtonian droplets. For example, polymeric droplets, which are relevant for technological applications and, also, often serve as simplified model systems for investigating biofluids, are among the most well studied in the case of complex fluids. Still, various results concerning the coalescence of polymeric droplets are contradictory in the literature, which calls for more research on the subject. On the one hand, for example, Dekker *et. al*, [37] have reported that the neck radius for coalescing (free hanging) polymer droplets follows the same temporal evolution as that of Newtonian droplets of very low viscosity, *i.e.*, $\beta = 0.5$, where β is an exponent expressing the temporal evolution of the neck radius. In this case, the presence of polymer chains was shown to affect the spatial features of coalescence. On the other hand, Verma *et.al* [38] reported a value of $\beta = 0.36$ for the evolution of the neck radius of a sessile – pendant droplet coalescence. Moreover, the value of β decreased even further for polymer concentrations roughly 20 times more than the critical concentration.

The coalescence of sessile polymeric droplets is relevant for many industrial applications such as microfluidics [39], spray coating [40], and 3D printing [41]. For coalescing droplets placed on a solid surface, the substrate introduces additional viscous stress. This viscous stress which depends on the wettability of the substrate and, can significantly affect the interactions. The coalescence dynamics can be quantified in terms of the temporal growth of the bridge width, r , and the bridge height, h . Similarl to the previous case, these two parameters grow in time as power laws which are expressed as follows: $r(t) \propto t^\beta$ and $h(t) \propto t^\alpha$. Dekker *et. al*, [37] has reported the same time evolution for bridge height as that of sessile inviscid Newtonian droplets ($\alpha = 2/3$). A departure from the Newtonian regime was observed only at very high polymer concentrations. Verma *et. al*, [42] studied the coalescence of polymeric fluid droplets on a partially wettable substrate, and a transition from $\alpha = 2/3$ to $\alpha = 1/2$ was observed with increasing polymer concentration. Arbabi *et. al*, [43] studied the coalescence of sessile polymeric droplets on a substrate with two different contact angles; 78° and 118° . The value of α was found to be greater at $\theta = 78^\circ$ than that in the case of $\theta = 118^\circ$, when all other parameters were kept the same. It was also observed that α decreases with increasing viscosity. For all the viscosities considered for both contact angles, the values of β were found to be less than 0.5 [43]. Rostami *et. al*, [44] have reported values of α and β for coalescing sessile viscoelastic droplets located

on a hydrophobic surface, for varying droplet elasticity. The value of α first decreases with increasing elasticity and reaches a minimum for the regime when both elasticity and viscosity play a role. When the elasticity increases further, the value of α increases again and reaches a plateau. All the reported values of α , again, were < 0.5 . Kaneelil *et. al.*, [45] have reported $\alpha \approx 1$ for two sessile viscoelastic droplets in the small contact-angle regime. This value was unaffected by varying the polymer concentration. Moreover, α was found to decrease gradually from an initial value of $\alpha = 2/3$ as the system moved from the viscosity dominant to the elasticity dominant regime. While most of these studies concern droplets coalescence on rigid substrates, only some of them have considered soft substrates. For example, Roy *et.al.*, [46] studied the coalescence of water droplets on a soft surface and has concluded that droplets exhibit reluctance to coalescence on these soft substrates. Sokuler *et. al.*, [47] also studied the merging of water droplets on a soft surface with increasing softness. They have reported similar results, namely, the relaxation time for drop shape after merging increases with increasing softness. They also observed that coalescence was prevented on surfaces, when the softness was higher than a threshold.

Viscoelastic droplets located on a soft surface is a common occurrence both in nature and technology. For soft surfaces the resting droplet may create deformations underneath, which, in turn, affects the coalescence. Furthermore, these deformations could be anisotropic and may lead to a directional motion of the droplet for a soft substrate with stiffness gradient [48, 49]. Such processes are also relevant in the context of cellular clusters. For example, they can migrate in a directional manner following the gradient in the mechanical properties of the substrate. Moreover, Understanding the behavior of multiple droplets moving on such deformable substrates may enhance our understanding about the fusion of cellular aggregates, which is an important step in morphogenesis, cancer metastasis and cell-based therapies [50, 51]. In addition, such a system setup may also be relevant for explaining the growth of microbial communities, on surfaces, through aggregate fusion under various conditions [10, 52, 53].

In this regard, we study the mutual interaction between two polymeric droplets that perform durotaxis motion on a gradient substrate [54]. Since the motion of the droplets takes place along the stiffness gradient, the interacting droplets essentially move in the same direction leading to a coupled interplay of droplet motion and coalescence on a substrate of varying wettability (stiffness) (Fig.1). We anticipate that our study not only enhances

understanding the fusion and growth of multicellular aggregates on a surface, but is also relevant for microfluidics, and biomedical applications [10, 55–58]. The manuscript is organized as following; in the section II, we discuss the system that is studied, in details and we describe the the computational method used to carry out the investigation. In next, we discuss the results in the section III which is followed section IV where we conclude the manuscript.

II. SYSTEM, MODEL AND METHODS

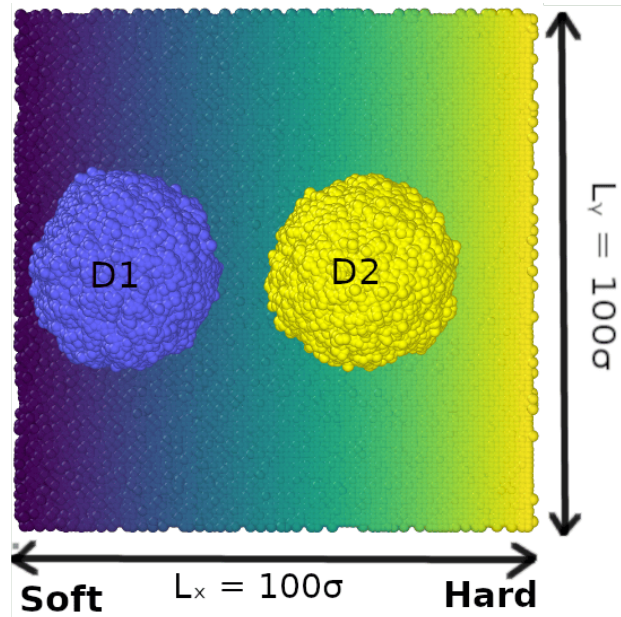


FIG. 1: System setup consisting of two polymer droplets marked as D_1 and D_2 , which are placed on a soft surface with stiffness gradient in positive x -direction as indicated by the color code and the arrow. In the case of stationary coalescence, the surface stiffness was kept uniform.

Our model is built on previous studies of the durotactic droplet motion of a polymer droplet on a surface with stiffness gradient, [49]. Here, our system consists of two polymer droplets placed on the substrate, while in the case of stationary coalescence the substrate stiffness was uniform. To simulate the coalescence between two droplets, which move in the same direction, a stiffness gradient was applied on the surface by using a harmonic potential as has been done previously [49]. This harmonic interaction potential reads

$$U_{harmonic}(r) = -\frac{1}{2}Kr^2, \quad (1)$$

where $r = 0$, when the bead is at its equilibrium position, and K is the spring constant, which is gradually changing to implement the stiffness gradient of the substrate. In particular, small values of K result in softer substrates (large thermal fluctuations of the beads) with the softness of the surface decreasing with increasing values of K . To create the gradient, the stiffness is increased by ΔK at every $\Delta L = 4\sigma$ (σ is the unit of length), starting from an initial value of K_0 . This increment takes place along the positive x -axis, starting from $x = 0$ to $x = 100\sigma$ (a top view of the system is presented in Fig.1) [49]. The linear dimensions of the substrate in both the x and the y directions are set to $L_x = L_y = 100\sigma$.

The droplets are made up of polymer chains, each containing 10 monomers. Consecutive monomers of each polymer chain are bonded by using the finite extensible nonlinear elastic (FENE) potential, which is mathematically expressed as follows:

$$U_{\text{FENE}}(r) = -\frac{1}{2}kR_0^2 \ln \left[1 - \left(\frac{r}{R_0} \right)^2 \right], \quad (2)$$

where r is the distance between two bonded monomers, $k = 30.0 \varepsilon/\sigma^2$ is the elastic constant, and $R_0 = 1.5\sigma$ the maximum bond extension. All non-bonded interactions between beads belonging to both the droplets and the substrate were modeled using the truncated and shifted Lennard-Jones (LJ) potential

$$U_{ij}(r_{ij}) = 4\varepsilon_{ij} \left[\left(\frac{\sigma_{ij}}{r_{ij}} \right)^{12} - \left(\frac{\sigma_{ij}}{r_{ij}} \right)^6 \right], \quad (3)$$

where, i and j stand for the type of monomer. d_1 denotes monomers making up the droplet D_1 , d_2 indicates the monomers belonging to droplet D_2 , while s stands for the monomers constituting the surface. r_{ij} is the distance between every interacting pair of beads within a cut-off distance, which is set to $r_c = 2.5\sigma$ for the droplet–droplet and the droplet–surface interactions, while $r_c = 2^{1/6}\sigma$ for the LJ interactions between the substrate beads. In the present study, we kept $\varepsilon_{ss} = \varepsilon_{d_1d_1} = \varepsilon$ fixed (ε is the energy unit), while ε_{d_1s} , ε_{d_2s} , $\varepsilon_{d_2d_2}$, and $\varepsilon_{d_1d_2}$ were varied to investigate the various scenarios.

The molecular dynamics (MD) simulations were conducted using LAMMPS package[59]. The Langevin thermostat, which was used here, includes random and dissipative forces to

the Newton's equation of motion for each bead, namely:

$$m \frac{d^2 \mathbf{r}_i}{dt^2} = -\nabla U_i - \gamma \frac{d\mathbf{r}_i}{dt} + \Gamma_i(t) \quad (4)$$

where $m = m$ is the mass of each monomer (all the monomers are of the same mass considering the same mass unit, m , for all cases), ∇U_i is the force acting on the i^{th} monomer due to the presence of all other beads within the cut-off distance, and γ is the damping coefficient set to $0.1\tau^{-1}$, where $\tau = (\frac{m\sigma^2}{\epsilon})^{1/2}$ is the time unit. The Langevin equation is integrated for each bead using the velocity-Verlet algorithm with time step $\delta t = 0.005\tau$. Γ is the random force on each bead representing the thermal fluctuations, and is related to γ via the fluctuations–dissipation theorem, namely

$$\langle \Gamma_i(t) \Gamma_j(t') \rangle = 6k_B T \gamma \delta_{ij} \delta(t - t'). \quad (5)$$

The dimensions of the simulation box are chosen large enough to avoid interactions with mirror images or the system, due to the presence of periodic boundary conditions in all three dimensions. Both droplets are equilibrated on the surface, keeping their mutual interaction off, for long enough such that the average shape of the droplets does not change with time. The droplets are placed along the stiffness gradient (positive x -axis) maintaining the distance between the last bead of the first droplet and the first bead of the last droplet to a value higher than 2.5σ (cutoff distance) after the equilibration. Once equilibrium was reached, the mutual interaction between the droplets was turned on. As a result, both droplets started moving due to the stiffness gradient, and subsequently are able to get close enough to start to interact or coalesce.

III. RESULTS

In this section, we present an analysis of the outcomes of the simulation runs for coalescence under varying system conditions. Temperature, FENE potential parameters, and the droplet size were kept fixed throughout the study. Temperature is set to be $T = 1.0 \epsilon/k_B$, the FENE potential parameters are fixed at $k = 30.0 \epsilon/\sigma^2$, and $R_0 = 1.5\sigma$. The coalescing droplets are both made up of 1800 polymers; each polymer contains 10 monomers. All the distances, in the following, are given in the units of σ and the potential parameters for well depth are in units of ϵ . We studied coalescence of stationary as well as moving droplets on a surface. For stationary coalescence, three different values of surface stiffness were considered. For the coalescence of moving droplets, the droplets were placed on a stiffness gradient

surface. The two droplets, then perform durotactic motion along the stiffness gradient and, somewhere on the way, these droplets meet and merge. This amounts to coalescence of two droplets moving in the same direction with trailing droplet moving with a higher speed than that of the leading droplet. A range of velocities ratio of trailing and leading droplets have been deployed to decode the effect of droplet’s motion on the coalescence.

Also, the strength of adhesion and inter-droplet cohesion was varied to gain an insight into the role of various intermolecular interactions on the process. In Fig. 1, we present the scheme of simulated system. There are two droplets, D_1 and D_2 , placed on a soft surface. For stationary coalescence, the substrate’s spring constant remains fixed throughout the surface. The stiffness of the surface increases with increasing K value, whereas the contact angle made by the droplet on surface decreases. In Table1, we have listed the values of θ_Y for each combination of K and ε .

A. Coalescence of stationary droplets on a soft surface

TABLE I: Dependence of contact angle on droplet–substrate interaction strength and substrate stiffness.

Interaction Strength (ε_{ds})	Substrate Stiffness ($k = \varepsilon/\sigma^2$)	Contact Angle ($\sim \theta^\circ$)
0.4	20	133°
	120	122°
	240	120°
0.5	20	122°
	120	110°
	240	106°
0.6	20	111°
	120	96°
	240	94°
0.7	20	97°
	120	82°
	240	80°

We first discuss the coalescence of D_1 and D_2 on uniform substrate’s stiffness for three different values of spring constant K , namely $K = 20$, $K = 120$ and $K = 240$. For all three cases, we kept $\varepsilon_{d_1s} = 0.7$ and $\varepsilon_{d_2s} = 0.40$ in the unit of ε . The values of contact angles for each combination of K, ε are given in Table I, where it can be seen that the contact angle (θ_Y)

decreases with increasing K and ε_{ds} . The values of θ_Y are approximated by fitting spherical caps to the droplets [60–64]. In the beginning of the simulation, centers of D_1 and D_2 are

$$K = 20$$

$$K = 240$$

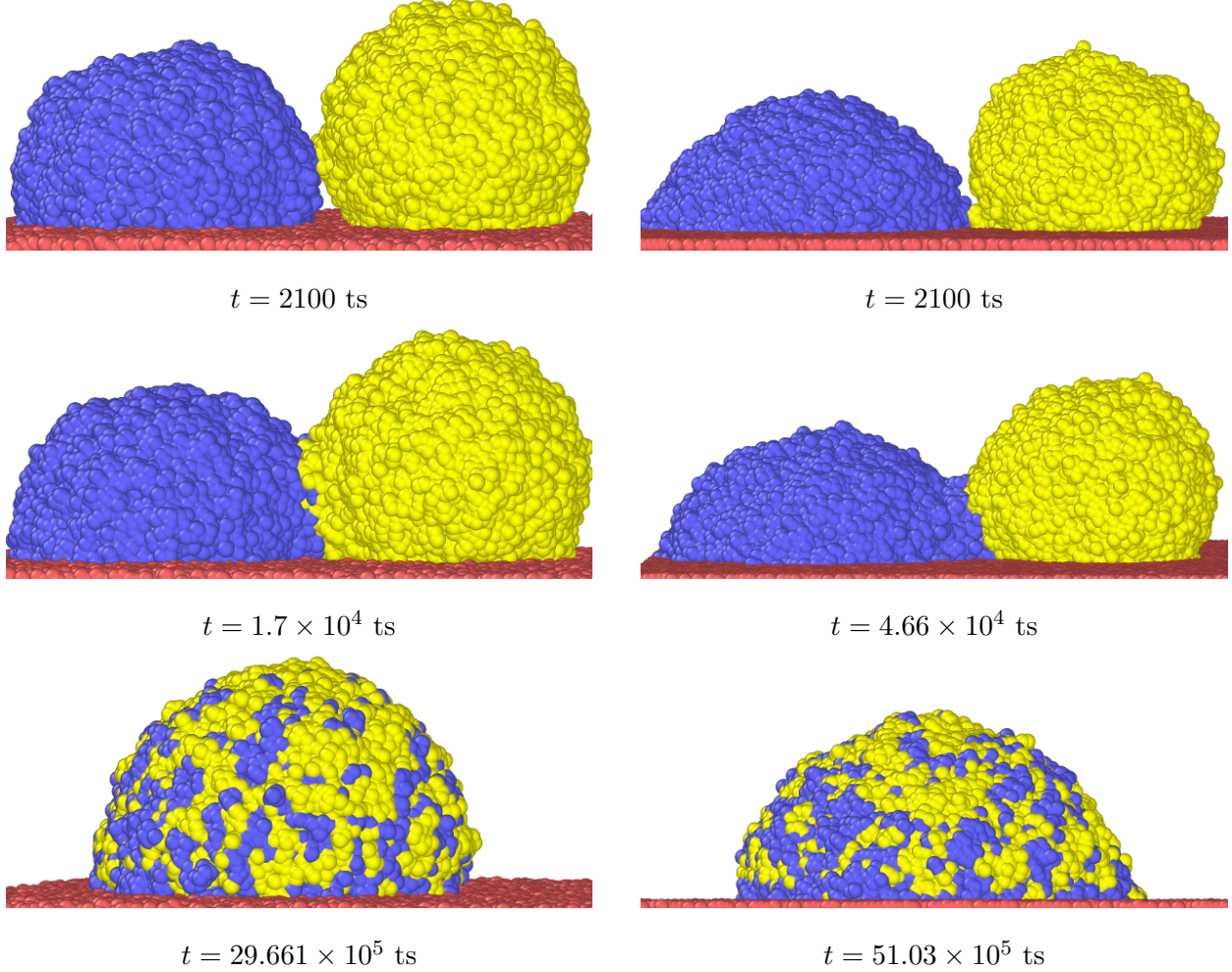


FIG. 2: Time evolution of droplet coalescence on a uniform substrate for different stiffness values. For left column, $K = 20$, and the substrate is softer than the one on the right column with $K = 240$. In the case of softer substrates the droplets are more spherical and the coalescence starts at the equator of the droplets, whereas for stiffer ones the droplets are more flat and the coalescence starts at the surface. Time is taken in units of timesteps (ts) and the origin is taken when the coalescence starts. The rest of the parameters are same as mentioned in Section III A.

placed such that the last beads of D_1 and first beads of D_2 are $\approx 10\sigma$ away. The droplets are equilibrated keeping their mutual interaction off *i.e.*, $\varepsilon_{d_1d_2} = 0$. Once equilibrated, the mutual interaction between the droplets is switched on and set to $\varepsilon_{d_1d_2} = 1.0$ for all the

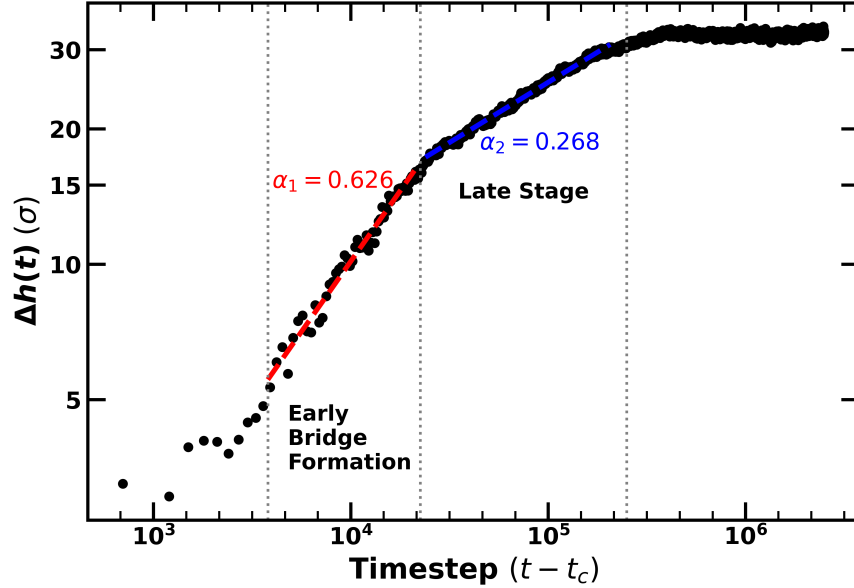


FIG. 3: Temporal evolution of bridge height for stationary coalescence on a surface with spring constant $K = 20$. The extracted power-law exponent has two values, namely $\alpha_1 = 0.626$ and $\alpha_2 = 0.268$, indicating a shift from a faster to a slower bridge growth as the coalescence progresses. The rest of the parameters are the same as mentioned in Sec. III A.

three K values. Overall, D_1 is attracted more to the surface than D_2 and hence acquires a flatter shape with smaller θ_Y .

For $K = 20$, the coalescence starts at the equator of the droplets as the droplets are more spherical and the beads at equators are the closest, namely within 2.5σ . The $D_1 - D_2$ interface, or the bridge forms at the equator and then grows vertically with time (Fig. 2). This temporal evolution of the bridge height, shown in Fig. 3, is one of the measures to quantify the coalescence dynamics. The bridge height follows a power-law growth in time before reaching a stable value. The power-law growth region consists of two regimes, where the bridge growth is faster in the early stages with a higher value of power-law exponent (α_1). The dynamics becomes considerably slower at a later stage as the system evolves over time and the corresponding value of the exponent, (α_2), decreases (Figure 3). Such a cross-over in dynamics is anticipated for viscoelastic droplets, since, in the beginning, the polymer chains follow the deformations caused by capillarity and contribute to the bridge growth. However, once the chains start to relax, the viscoelastic resistance slows down the bridge growth [43, 44, 65].

For $K = 20$, $\alpha_1 = 0.6260$ and $\alpha_2 = 0.2679$. The values of α_1 decrease with increasing K , whereas, α_2 increases (values are listed in Table II). The variation of α_1 with $K(\theta_Y)$ can be understood in terms of competition between the droplet–droplet and droplet–surface attractions. For $K = 20$, the droplet–surface attraction is weaker and the coalescence starts a few molecular diameters away from the substrate. Thus, the competing attraction from the surface, which essentially pulls the polymers forming bridge towards itself, is less effective. As K increases, the surface–droplet attraction increases for both droplets, thus the droplets spreading more. The coalescence starts on the surface as well. This stronger attraction competes with the bridge growth in the vertical direction, thus reducing the values of α_1 . In the second regime of the bridge growth, this trend is reversed, *i.e.*, the value of α_2 is the smallest for $K = 20$ and increases with K . In this regime, the viscoelastic relaxation of the polymers is at work, trying to bring the stretched polymers back to equilibrium. In such a scenario, the droplet–surface attraction counters this viscoelastic resistance, and, thus, further favors the bridge growth. This implies that a higher droplet–surface attraction would lead to faster bridge growth in the second regime.

As mentioned in Section I, a few studies have thus far been conducted on the coalescence of sessile polymer droplets, including polymer solution droplets. Moreover, the reported values of α vary from one study to another, although all these studies report $\alpha < 0.5$ in the case of coalescence on partially wettable surfaces. $\alpha > 0.5$ was only reported for the cases where either the polymer concentration, or the contact angle is very small [37, 43–

TABLE II: Scaling exponents (α_1, α_2) describing the time evolution of the bridge height, $h(t) \sim t^\alpha$, for varying substrate stiffness k at fixed droplet–surface interaction parameters $(\varepsilon_{d_1s}, \varepsilon_{d_2s}) = (0.7, 0.4)$. The early time exponent α_1 is associated with the early bridge formation regime, while the exponent α_2 corresponds to the late vertical growth of the interfacial contact region. Uncertainties denote the standard error of the mean.

k	Bridge formation (early) α_1	Interfacial growth (late) α_2
20	0.6260 ± 0.0066	0.2679 ± 0.0006
120	0.4412 ± 0.0041	0.2899 ± 0.0007
240	0.4266 ± 0.0020	0.3089 ± 0.0008

45]. Results presented in our study are comparable to the values reported in the literature, especially the values of α_2 . It is to be emphasized here that, for viscoelastic fluids, two different regimes should exist as a signature of the crossover from the capillarity-dominated to the viscoelasticity-dominated regime [44].

B. Coalescence of moving droplets

With the understanding unfolded in the last section, we now turn our attention to the coalescence of two droplets that perform durotactic motion in the same direction on a gradient surface (Fig. 1). To create the gradient surface, the initial value of the stiffness is set to be $K = 20$ at $x = 0$, and is increased by $\Delta K = 10.666$ every 4σ in the positive x -direction. In response to the gradient, the droplets move from the softer to the stiffer edge of the substrate. The speed of the droplets depends on the strength of the droplet-substrate interaction, *i.e.*, ε_{d_1s} and ε_{d_2s} . Overall, higher interactions yield higher speeds. The rest of the system parameters are set to $\varepsilon_{d_1s} = 0.7$, $\varepsilon_{d_2s} = 0.4$, and $\varepsilon_{d_1d_1} = \varepsilon_{d_2d_2} = \varepsilon_{d_1d_2} = 1.0$. $\varepsilon_{d_1s} > \varepsilon_{d_2s}$ ensures that the trailing droplet meets the leading one before reaching the end of the substrate.

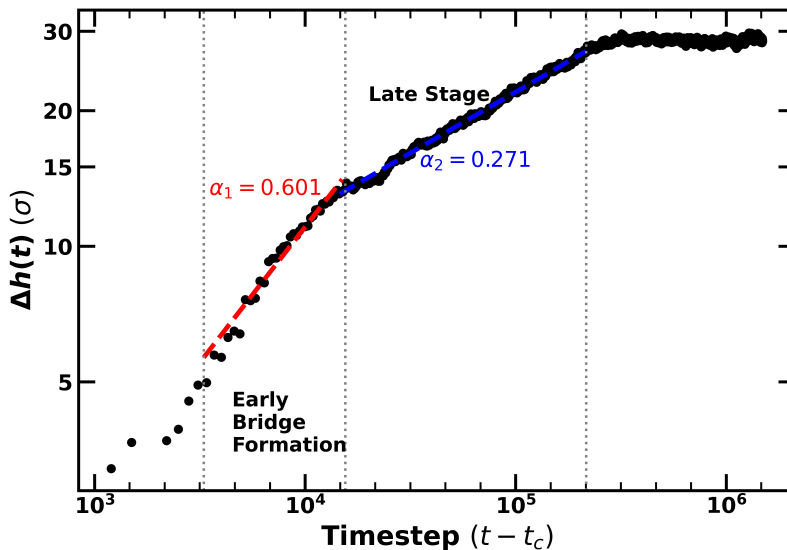


FIG. 4: Temporal evolution of bridge height for the coalescence of two droplets moving on a gradient surface with $\varepsilon_{d_1s} = 0.70$ and $\varepsilon_{d_2s} = 0.40$. The rest of the interaction parameters are same as mentioned in the Sec. III B. The bridge height, again, has two regimes of power law growth before attaining a stable value.

TABLE III: Scaling exponents α describing the time evolution of the bridge height, $h(t) \sim t^\alpha$, for varying substrate interaction pairs $(\varepsilon_{d_1s}, \varepsilon_{d_2s})$.

$(\varepsilon_{1s}, \varepsilon_{2s})$	Bridge formation (early) α_1	Interfacial growth (late) α_2
(0.7, 0.4)	0.6013 ± 0.0108	0.2707 ± 0.0004
(0.6, 0.4)	0.6342 ± 0.0097	0.2653 ± 0.0019
(0.5, 0.4)	0.6509 ± 0.0079	0.2454 ± 0.0015
(0.4, 0.4)	0.6742 ± 0.0046	0.2329 ± 0.0004
(0.7, 0.5)	0.5220 ± 0.0038	0.3118 ± 0.0008
(0.6, 0.5)	0.5307 ± 0.0065	0.3092 ± 0.0004
(0.5, 0.5)	0.5972 ± 0.0053	0.2750 ± 0.0004

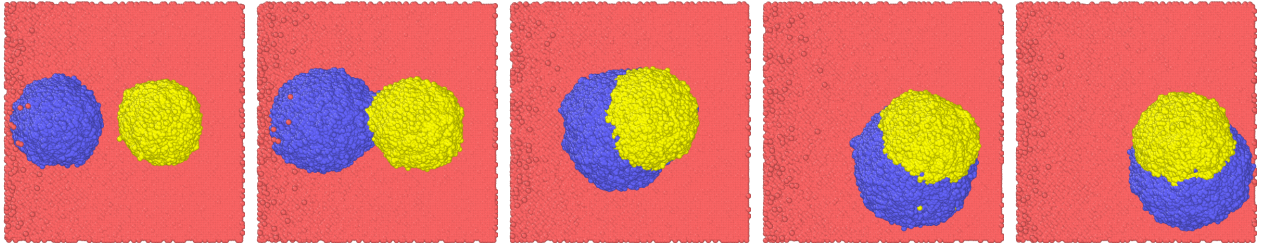
In the beginning of the simulation, the center of D_1 is placed at $(x = 20, y = 50, z = 18)$ and the center of D_2 is placed at $(x = 68, y = 50, z = 18)$. The droplets are again equilibrated while keeping their mutual interaction off. Once, the system reached equilibrium, $\varepsilon_{d_1d_2}$ is set to 1.0 and both droplets start moving in the positive x - direction. Since $\varepsilon_{d_1s} > \varepsilon_{d_2s}$, D_1 (trailing droplet) moves faster than the leading droplet D_2 . As a result, on the way both droplets come close enough to come in to physical contact with each other. In this case, the bridge starts forming at the substrate and it then grows in the vertical direction. Since the droplets are fully miscible, the $D_1 - D_2$ interface moves inside D_2 as the mixing progresses and the end product is a homogeneous mixture of D_1 and D_2 particles. Throughout the mixing, the the two droplets continue to move as one entity along the gradient.

The temporal evolution of the bridge height is shown in Fig 4. In this case, the values of the power-law exponents are $\alpha_1 = 0.601 \pm 0.016$, and $\alpha_2 = 0.270 \pm 0.001$ (Figure 4). These values are much closer to the power-law exponent reported in the case of stationary coalescence at $K = 20$, but they are still substantially higher than those at $K = 120$ and $K = 240$, the physical location of the coalescence corresponds to the values of K closer to 240 though. This increase in α_1 and α_2 may be attributed to the momentum (inertia) that D_1 brings with it. In order to understand the coalescence of moving droplets better, we varied the relative speeds of D_1 and D_2 . First, the value of ε_{d_1s} was reduced keeping $\varepsilon_{d_2s} = 0.40$. Decreasing ε_{d_1s} has two effects, that is the speed of D_1 reduces, and at the same time, the

D_1 -surface attraction also becomes lower. As we observed in the stationary coalescence, α_1 increases with decreasing droplet–surface attraction, whereas the value of α_2 decreases. The droplet–surface attraction in the first regime acts against the capillary force thus driving the bridge formation, whereas in the second regime it acts against the viscoelastic resistance thus helping in the bridge formation. This trend is also seen here: when the velocity of D_1 (ε_{d_1s}) decreases while keeping ε_{d_2s} fixed, α_1 increases and α_2 decreases. In the case of $\varepsilon_{d_1s} = \varepsilon_{d_2s} = 0.4$, *e.g.*, the coalescence starts at the equator of the droplet, the value of α_1 is largest reaches its maximum in this case while α_2 acquires its lowest value.

When the attraction of D_2 with the surface increased to $\varepsilon_{d_2s} = 0.50$ while keeping $\varepsilon_{d_1s} = 0.70$, the value of α_1 decreases, whereas the value of α_2 increases (Table III). This follows exactly the opposite trend to the previous case, when velocity of D_1 decreased. The slowdown in the first regime might be attributed to the reduced relative velocity with which D_1 impacts D_2 at the contact, thus pushing the bridge inside the D_2 . In the second regime, the increased D_2 –surface attraction drives a faster bridge growth. The bridge height was found to be maximum for the case of ($\varepsilon_{d_1s} = \varepsilon_{d_2s} = 0.40$), because both droplets maintained a more spherical shape in this case in comparison with the other cases.

C. Effect of varying $\varepsilon_{d_1d_2}$



$t = 1.2 \times 10^5$ ts $t = 5.66 \times 10^5$ ts $t = 2.87 \times 10^6$ ts $t = 2.29 \times 10^7$ ts $t = 3.85 \times 10^7$ ts

FIG. 5: Time-sequenced images of coalescence of two moving droplets for $\varepsilon_{d_1d_2} = 0.85$. As can be seen, the trailing droplet tries to bypass the leading one, and the combined entity rotates anti-clockwise. The torque is generated because the the surface– D_1 attraction is stronger than $D_1 - D_2$ attraction. Sec. III C

In this section, we focus our attention on the coalescence of moving droplets as a function of $\varepsilon_{d_1d_2}$, which has been varied in the range 1.0 – 0.30. Other parameters were set to

$\varepsilon_{d_1} = \varepsilon_{d_2} = 1.0$, $\varepsilon_{d_1s} = 0.70$ and $\varepsilon_{d_2s} = 0.40$. For $\varepsilon_{d_1d_2} = 1.0$, the droplets mix completely as we have seen in the previous section. In Fig 5, we present the time-sequenced snapshots for the coalescence for $\varepsilon_{d_1d_2} = 0.85$. In this case, the coalescence does not proceed via a bridge formation. Instead, the D_1 prefers to continue along the stiffness gradient as $\varepsilon_{d_1s} > \varepsilon_{d_1d_2}$. D_2 , being significantly slower, rather acts like an obstacle, which D_1 tries to bypass either from the left or from the right. The part of D_1 that is closer to D_2 starts to mix with D_2 with a layer of D_1 forming between D_2 and the surface. The combined effect results in a final product that looks like D_2 partly scooped in D_1 (Figure 5).

The value of $\varepsilon_{d_1d_2}$ was decreased further, the next value considered was 0.75. A large $D_1 - D_2$ interface still forms, but there is no layer of D_1 between D_2 and the surface as the attraction between D_1 and D_2 decreases. The combined body still feels a torque as the part of D_1 that does not make interface with D_2 moves faster and tries to overtake D_2 from either left or right. With decreasing $\varepsilon_{d_1d_2}$, however, the $D_1 - D_2$ contact area reduces and so does the applied torque. In Fig. 6a, we show the temporal evolution of ΔR (distance between the centers of mass of D_1 and D_2) for varying values of $\varepsilon_{d_1d_2}$. The distance between the two centers of mass increases with decreasing $\varepsilon_{d_1d_2}$. The x and y components of ΔR also increase with decreasing $\varepsilon_{d_1d_2}$, but the z component varies differently: Δz is the maximum for $\varepsilon_{d_1d_2} = 0.85$ and then decreases when $\varepsilon_{d_1d_2}$ decreases further (Fig.6b). For $\varepsilon_{d_1d_2} = 0.85$, a

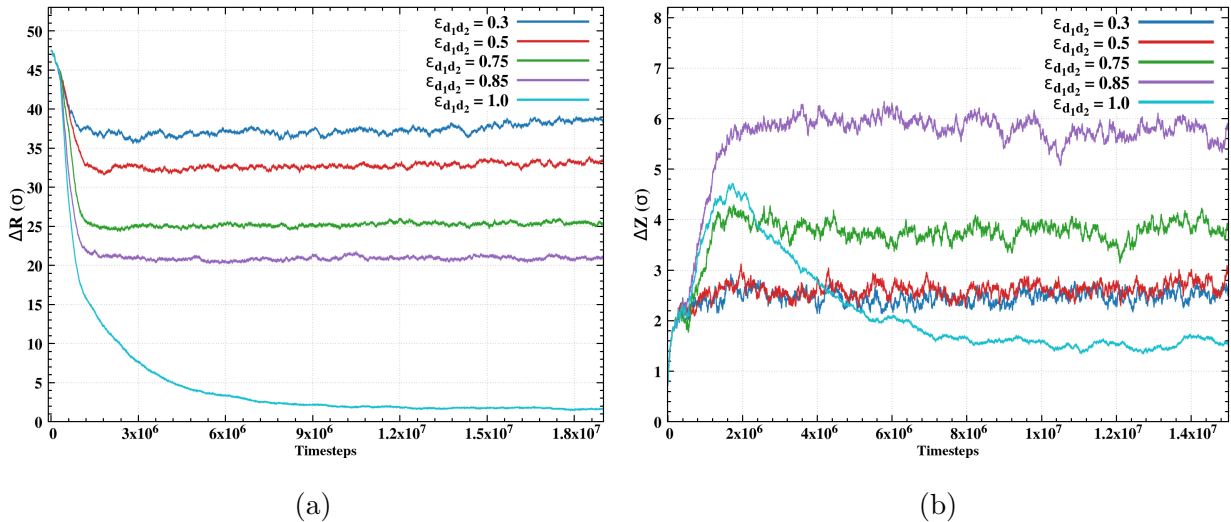


FIG. 6: Difference of centers of mass of the coalescing droplets (ΔR) and z - component thereof (Δz) for different $\varepsilon_{d_1d_2}$, other system parameters are the same as mentioned in

Sec. III C

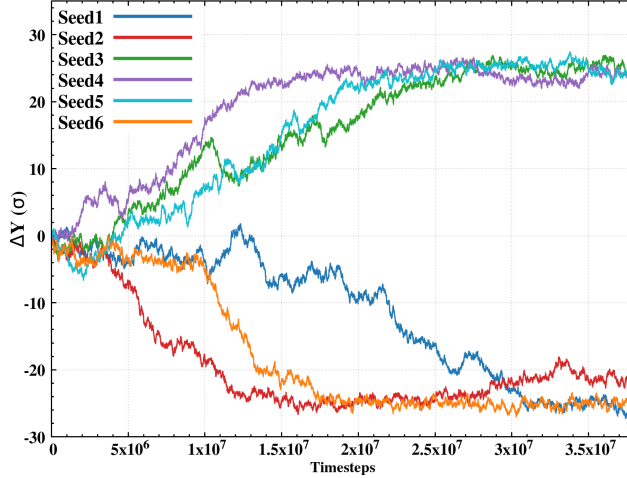


FIG. 7: y -component of ΔR for different independent runs, showing that the probability of D_1 trying to pass D_2 from left and right are equal. The rest is the same as in Fig. 6a.

part of D_1 slides in between the D_2 and the substrate, but, when $\varepsilon_{d_1 d_2}$ is decreased further, $D_1 - D_2$ interface starts shrinking and the z -coordinates of the centers of mass of the droplets align more and more. The possibility of D_1 trying to pass D_2 from the right is equal to that of D_1 passing from the left, as there is no force favoring one direction over the other. The same can be seen in the difference between y -coordinates of the centers of mass of D_1 and D_2 (ΔY) for different independent runs, as shown in Fig 7.

D. Effect of varying ε_{d_2}

In this section, the strength of attraction between the particles comprising $D_2(\varepsilon_{d_2 d_2})$ was varied keeping $\varepsilon_{d_1 d_1} = \varepsilon_{d_1 d_2} = 1.0$, $\varepsilon_{d_1 s} = 0.70$, and $\varepsilon_{d_2 s} = 0.40$. When $\varepsilon_{d_2 d_2}$ is decreased from 1.0 to 0.90 and 0.80, the coalescence becomes faster and the droplets mix to a higher degree. This can be seen in terms of the distance between the centers of mass of the two droplets (ΔR , Fig. 8). The droplets also move along the stiffness gradient while coalescing. When $\varepsilon_{d_2 d_2}$ was increased beyond 1.0, the coalescence is impeded. Now, the attraction between D_2 particles is stronger than that between the particles of D_1 , as well as between the particles of D_1 and D_2 , so the mixing is no more uniform. The particles belonging to D_2 droplet try to stay together. As a result, the droplet moves in a way that it keeps its structure inside D_1 as illustrated by the partial mixing inside the envelope of D_1 . With increasing $\varepsilon_{d_2 d_2}$, the depth of the D_1 envelope on D_2 becomes smaller as the degree of mixing decreases,

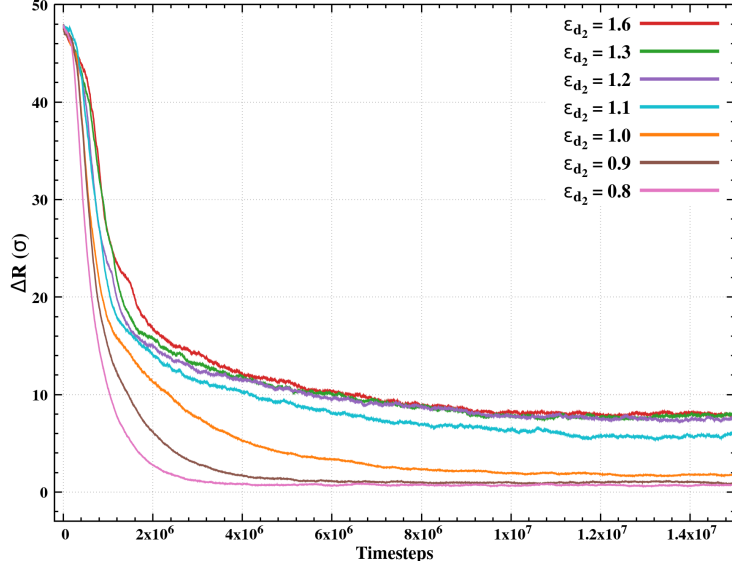
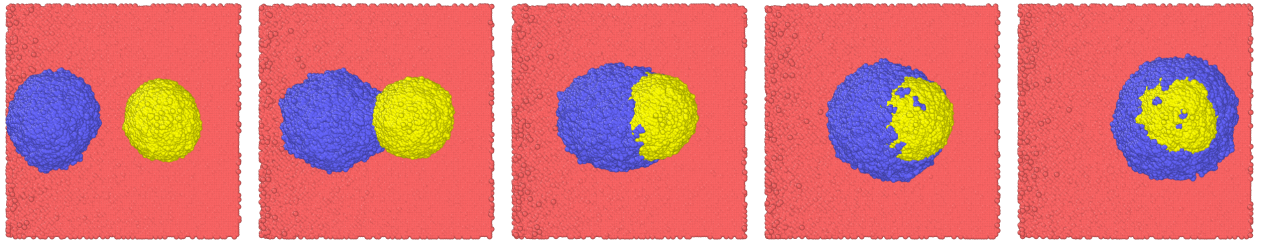


FIG. 8: Distance between centers of mass of two coalescing droplets on a gradient surface for varying $\varepsilon_{d_2 d_2}$. As can be seen the distance between the two centers of mass increases with increasing $\varepsilon_{d_2 d_2}$ indicating a decreasing mixing. Rest of the parameters are same as mentioned in the Sec. III D



$t = 1.68 \times 10^5$ ts $t = 8.62 \times 10^5$ ts $t = 1.114 \times 10^6$ ts $t = 1.796 \times 10^6$ ts $t = 1.16 \times 10^7$ ts

FIG. 9: Time sequenced snapshot for coalescence of moving droplets for $\varepsilon_{d_2} = 1.6$. The other parameters are given in Sec. III D

due to the increased attraction between the D_2 particles. This, again, is reflected in ΔR , which increases with increasing $\varepsilon_{d_2 d_2}$ (Fig. 8). In Fig. 9, the time-sequenced snapshots for $\varepsilon_{d_1 d_2} = 1.6$ are presented to provide a better understanding of the final product when the inter-droplet attraction of one droplet is much stronger than the inter-droplet attraction of the other droplet.

IV. SUMMARY AND FUTURE OUTLOOK

In this manuscript, we have studied the coalescence of polymeric droplets on a soft surface, by means of molecular dynamics simulation of a coarse-grained model. First, we studied the coalescence of two stationary droplets on a soft surface without stiffness gradient for three different values of “surface-softness”. The coalescence dynamics were characterized by analyzing the temporal growth of the bridge height, which unlike Newtonian fluids, exhibits two distinct regimes of power-law dependence. A faster bridge growth, in the beginning, is followed by a slower growth before attaining a constant value. The slowdown of the dynamics in the second regime might be attributed to the emergence of viscoelastic relaxation of the polymer chains. The bridge height grows the fastest in the first regime for the softest surface and slows down with increasing stiffness. In the second regime, the trend is reversed, *i.e.*, the rate of the bridge growth increases with increasing stiffness. This may be understood in terms of the competition between the droplet–droplet attraction, the droplet–surface attraction and the viscoelastic relaxation. Then, a stiffness gradient was created on the surface and the droplets were initially kept sufficiently apart. The droplets undergo durotactic motion in response to the gradient, moving from the softer to the stiffer end of the substrate. The velocity of the droplets depends on the droplet–surface attraction: ε_{d_1s} and ε_{d_2s} are chosen such that the trailing droplet moves with a higher velocity in comparison with the leading droplet. On the way, when the droplets come close enough to interact, coalescence starts with the combined entity continuing the durotactic motion. The dynamics and the extent of the coalescence depend on a number parameters, which will be summarized in the following.

The speed of coalescing droplets was varied and it was found that decreasing the velocity of the trailing droplet favors the bridge growth in the first regime, whereas it slows it down in the second regime. The opposite effect was observed when increasing the velocity of D_2 , *i.e.*, the bridge height growth becomes slower in the first regime and faster in the second regime. This may, again, be understood in terms of the competition between capillary forces, viscoelastic resistance, and relative momentum of the moving droplets. A slower D_1 in the beginning means smaller relative momentum, but, also, a weaker D_1 – surface attraction to compete with the $D_1 - D_2$ attraction. In contrast, in the second regime, a weaker D_1 – surface attraction reflects a weaker competition to the chain relaxation. Similarly, a faster D_2 or a higher value of ε_{d_2s} means the particles forming bridge will feel more attracted to the

surface and hence the bridge growth slows down, in the first regime. In the second regime, higher ε_{d_2s} will oppose viscoelastic relaxation, leading to a faster growth.

In addition, the strength of the inter-droplet interaction was varied. When $\varepsilon_{d_1d_2}$ was increased beyond $\varepsilon_{d_1d_1} = \varepsilon_{d_2d_2} = 1.0$, the coalescence becomes faster and the droplets mix better. However, when $\varepsilon_{d_1d_2}$ was decreased below $\varepsilon_{d_1} = \varepsilon_{d_2d_2} = 1.0$, the droplets mix up to a certain degree. In particular, the degree of mixing decreases with decreasing $\varepsilon_{d_1d_2}$. The combined body of the two droplets also experiences torque while coalescing and moving at the same time. So far, the value of $\varepsilon_{d_1d_1}$ was kept equal to $\varepsilon_{d_2d_2}$. When $\varepsilon_{d_2d_2}$ was taken to be greater than $\varepsilon_{d_1d_1}$ and $\varepsilon_{d_1d_2}$, the coalescence exhibits a slightly different behavior. The D_1 droplet, while coalescing with D_2 , also envelops D_2 . Since the attraction between D_2 particles is stronger than that between D_1 particles and the attraction between $D_1 - D_2$ particles, the D_2 opposes mixing. The envelope is created by the D_1 particles, which are pulled into D_2 , due to capillary forces. Both the extent of mixing and enveloping decrease with increasing $\varepsilon_{d_2d_2}$.

Apart from engineering applications, the findings of this study may carry relevance for our fundamental understanding of biological processes, particularly in the context of fusion of multicellular aggregates, which plays an important role in development, disease, and therapy. The demonstration that durotaxis-driven coalescence of viscoelastic droplets produces qualitatively distinct morphological outcomes — complete mixing, partial enveloping, or bypass — depending on the ratio of the inter- and intra-droplet cohesion maps naturally onto the collective behavior of cell clusters whose intercellular adhesion strength differs between cluster types. The enveloping morphology, in particular, draws a parallel with the engulfment of mechanically stiffer tumor spheroids by softer stromal or immune cell aggregates. It is also worth mentioning here that fusion of cellular aggregates during morphogenesis the fusion exhibits two regimes: an initial rapid contact followed by a much slower, relaxation-limited integration, which is sensitive to the mechanical properties of the substrate.

We anticipate that the results of this study may offer new insights into the coalescence of viscoelastic droplets on soft substrates. However, there is still a lot to be explored when it comes to the coalescence of non-Newtonian fluids, coalescence on soft surfaces, or coalescence of moving droplets. It would be interesting, for example, to study the effect of bending rigidity of the droplets on the coalescence. Another aspect, that is relevant for microfluidics as well as in a biological context is to study the coalescence of viscoelastic fluids in confined

geometries, such as micro-channels or a Hele-Shaw geometry.

ACKNOWLEDGMENT

DT, VK and SLS acknowledge the generous financial support received from BHU under the IoE scheme and from SERB, New Delhi. DT and SLS also thank CSIR, New Delhi for financial support (grant id: 03WS-012-2023-24-EMR-II).

-
- [1] Y. Li, A. A. Pahlavan, Y. Chen, S. Liu, Y. Li, H. A. Stone, and S. Granick, *Proceedings of the National Academy of Sciences* **120**, [10.1073/pnas.2214657120](https://doi.org/10.1073/pnas.2214657120) (2023).
 - [2] T. Xiao, X. Ma, H. Hu, F. Xiang, X. Zhang, Y. Zheng, H. Dong, B. Adhikari, Q. Wang, and A. Shi, *Food Chemistry: X* **29**, 102792 (2025).
 - [3] C. L. Tucker, III and P. Moldenaers, *Annual Review of Fluid Mechanics* **34**, 177 (2002).
 - [4] J. Kamp, J. Villwock, and M. Kraume, *Reviews in Chemical Engineering* **33**, 1–47 (2016).
 - [5] I. Sarig, Y. Starosvetsky, and A. D. Gat, *Journal of Fluid Mechanics* **800**, 264–277 (2016).
 - [6] T. K. Pradhan and P. K. Panigrahi, *Colloids and Surfaces A: Physicochemical and Engineering Aspects* **608**, 125555 (2021).
 - [7] B. Hafskjold, T. B. Morrow, H. K. B. Celius, and D. R. Johnson, in *SPE Annual Technical Conference and Exhibition*, 94SPE (SPE, 1994).
 - [8] A. D. Pizarro, C. L. A. Berli, G. J. A. A. Soler-Illia, and M. G. Bellino, *Nature Communications* **13**, [10.1038/s41467-022-30834-2](https://doi.org/10.1038/s41467-022-30834-2) (2022).
 - [9] C. H. Meredith, P. G. Moerman, J. Groenewold, Y.-J. Chiu, W. K. Kegel, A. van Blaaderen, and L. D. Zarzar, *Nature Chemistry* **12**, 1136–1142 (2020).
 - [10] W. Pönisch, C. A. Weber, G. Juckeland, N. Biais, and V. Zaburdaev, *New Journal of Physics* **19**, 015003 (2017).
 - [11] R. A. Foty and M. S. Steinberg, *Developmental Biology* **278**, 255–263 (2005).
 - [12] D. Oriola, M. Marin-Riera, K. Anlaş, N. Gritti, M. Sanaki-Matsumiya, G. Aalderink, M. Ebisuya, J. Sharpe, and V. Trivedi, *Soft Matter* **18**, 3771–3780 (2022).
 - [13] S. Sart, A.-C. Tsai, Y. Li, and T. Ma, *Tissue Engineering Part B: Reviews* **20**, 365–380 (2014).

- [14] P. W. Oakes, D. C. Patel, N. A. Morin, D. P. Zitterbart, B. Fabry, J. S. Reichner, and J. X. Tang, *Blood* **114**, 1387–1395 (2009).
- [15] N. Jain, J. Moeller, and V. Vogel, *Annual Review of Biomedical Engineering* **21**, 267–297 (2019).
- [16] W. Li, X. Tang, and L. Wang, *Science Advances* **6**, 10.1126/sciadv.abc1693 (2020).
- [17] G. M. Whitesides, E. Ostuni, S. Takayama, X. Jiang, and D. E. Ingber, *Annual Review of Biomedical Engineering* **3**, 335–373 (2001).
- [18] H. Geng, J. Feng, L. M. Stabryla, and S. K. Cho, *Lab on a Chip* **17**, 1060–1068 (2017).
- [19] H. Zhao, D. Orejon, K. Sefiane, and M. E. R. Shanahan, *Langmuir* **41**, 3986–3994 (2025).
- [20] J. Eggers, J. E. Sprittles, and J. H. Snoeijer, *Annual Review of Fluid Mechanics* **57**, 61 (2025).
- [21] J. EGGERS, J. R. LISTER, and H. A. STONE, *Journal of Fluid Mechanics* **401**, 293–310 (1999).
- [22] J. Eggers, J. E. Sprittles, and J. H. Snoeijer, *Annual Review of Fluid Mechanics* **57**, 61–87 (2025).
- [23] H. Yue, J. C. Burton, and D. M. Sussman, *Physical Review Research* **6**, 10.1103/physrevresearch.6.023115 (2024).
- [24] A. Menchaca-Rocha, A. Martínez-Dávalos, R. Núñez, S. Popinet, and S. Zaleski, *Physical Review E* **63**, 10.1103/physreve.63.046309 (2001).
- [25] S. Ryu, H. Zhang, and U. J. Anuta, *Micromachines* **14**, 2046 (2023).
- [26] H. P. Kavehpour, *Annual Review of Fluid Mechanics* **47**, 245–268 (2015).
- [27] D. G. A. L. Aarts, H. N. W. Lekkerkerker, H. Guo, G. H. Wegdam, and D. Bonn, *Physical Review Letters* **95**, 10.1103/physrevlett.95.164503 (2005).
- [28] V. Arumugam and A. Vasudevan, in *4TH INTERNATIONAL CONFERENCE ON ROBOTICS, INTELLIGENT AUTOMATION AND CONTROL TECHNOLOGIES (RI-ACT2023)*, Vol. 3216 (AIP Publishing, 2024) p. 030001.
- [29] R. W. Hopper, *Journal of the American Ceramic Society* **67**, C-262 (1984), <https://ceramics.onlinelibrary.wiley.com/doi/pdf/10.1111/j.1151-2916.1984.tb19692.x>.
- [30] R. W. Hopper, *Journal of Fluid Mechanics* **213**, 349–375 (1990).
- [31] L. DUCHEMIN, J. EGGERS, and C. JOSSERAND, *Journal of Fluid Mechanics* **487**, 167–178 (2003).

- [32] J. D. Paulsen, J. C. Burton, S. R. Nagel, S. Appathurai, M. T. Harris, and O. A. Basaran, *Proceedings of the National Academy of Sciences* **109**, 6857–6861 (2012).
- [33] N. K. Chandra and A. Kumar, *Soft Matter* **21**, 3168–3183 (2025).
- [34] J. D. Paulsen, J. C. Burton, and S. R. Nagel, *Physical Review Letters* **106**, [10.1103/physrevlett.106.114501](https://doi.org/10.1103/physrevlett.106.114501) (2011).
- [35] J. D. Paulsen, *Physical Review E* **88**, [10.1103/physreve.88.063010](https://doi.org/10.1103/physreve.88.063010) (2013).
- [36] A. U. Joshi, O. A. Basaran, and D. S. Corti, *Physical Review E* **111**, [10.1103/fpb9-pbcc](https://doi.org/10.1103/fpb9-pbcc) (2025).
- [37] P. J. Dekker, M. A. Hack, W. Tewes, C. Datt, A. Bouillant, and J. H. Snoeijer, *Physical Review Letters* **128**, [10.1103/physrevlett.128.028004](https://doi.org/10.1103/physrevlett.128.028004) (2022).
- [38] S. C. Varma, A. Saha, S. Mukherjee, A. Bandopadhyay, A. Kumar, and S. Chakraborty, *Soft Matter* **16**, 10921–10927 (2020).
- [39] M. R. Hassan, J. Zhang, and C. Wang, *Langmuir* **37**, 5823–5837 (2021).
- [40] D. Lohse, *Annual Review of Fluid Mechanics* **54**, 349–382 (2022).
- [41] A. Klestova, E. Sergeeva, and A. V. Vinogradov, *Coatings* **9**, 275 (2019).
- [42] S. C. Varma, A. Saha, and A. Kumar, *Physics of Fluids* **33**, [10.1063/5.0073936](https://doi.org/10.1063/5.0073936) (2021).
- [43] S. Arbabi and P. E. Theodorakis, *Macromolecular Theory and Simulations* **32**, [10.1002/mats.202300017](https://doi.org/10.1002/mats.202300017) (2023).
- [44] P. Rostami, A. Erb, R. Azizmalayeri, J. Steinmann, R. W. Stark, and G. K. Auernhammer, *Physical Review Fluids* **10**, [10.1103/physrevfluids.10.063603](https://doi.org/10.1103/physrevfluids.10.063603) (2025).
- [45] P. R. Kaneelil, K. Tojo, P. K. Farsoiya, L. Deike, and H. A. Stone, *Journal of Fluid Mechanics* **1026**, [10.1017/jfm.2025.10878](https://doi.org/10.1017/jfm.2025.10878) (2026).
- [46] R. Roy, R. L. Seiler, J. A. Weibel, and S. V. Garimella, *Advanced Materials Interfaces* **7**, [10.1002/admi.202000731](https://doi.org/10.1002/admi.202000731) (2020).
- [47] M. Sokuler, G. K. Auernhammer, M. Roth, C. Liu, E. Bonaccorso, and H.-J. Butt, *Langmuir* **26**, 1544–1547 (2009).
- [48] R. Kajouri, P. E. Theodorakis, and A. Milchev, *Langmuir* **40**, 17779–17785 (2024).
- [49] P. E. Theodorakis, S. A. Egorov, and A. Milchev, *The Journal of Chemical Physics* **146**, [10.1063/1.4990436](https://doi.org/10.1063/1.4990436) (2017).
- [50] M. Palmiero, I. Cantarosso, L. di Blasio, V. Monica, B. Peracino, L. Primo, and A. Puliafito, *Molecular Oncology* **17**, 1699–1725 (2023).

- [51] J. Kim and T. Ma, *Biotechnology Progress* **29**, 441–451 (2013).
- [52] R. Porter, C. Trenado-Yuste, A. Martinez-Calvo, M. Su, N. S. Wingreen, S. S. Datta, and K. C. Huang, *Nature Reviews Physics* [10.1038/s42254-025-00849-x](https://doi.org/10.1038/s42254-025-00849-x) (2025).
- [53] A. Welker, T. Cronenberg, R. Zöllner, C. Meel, K. Siewering, N. Bender, M. Hennes, E. R. Oldewurtel, and B. Maier, *Physical Review Letters* **121**, [10.1103/physrevlett.121.118102](https://doi.org/10.1103/physrevlett.121.118102) (2018).
- [54] P. E. Theodorakis and A. Milchev, *Advances in Colloid and Interface Science* **353**, 103882 (2026).
- [55] H. Zhu, Q. Deng, J. Li, L. Yang, H. Li, Z. Zhao, Z. Wang, C. Pang, Y. Zhang, V. C.-H. Lui, W. Li, X. Yin, and L. Wang, *Science Advances* **11**, [10.1126/sciadv.adv6314](https://doi.org/10.1126/sciadv.adv6314) (2025).
- [56] M. Alistar and U. Gaudenz, *Bioengineering* **4**, 45 (2017).
- [57] S. K. Cho, H. Moon, and C.-J. Kim, *Journal of Microelectromechanical Systems* **12**, 70–80 (2003).
- [58] M. Knoche, *Crop Protection* **13**, 163–178 (1994).
- [59] A. P. Thompson, H. M. Aktulga, R. Berger, D. S. Bolintineanu, W. M. Brown, P. S. Crozier, P. J. in 't Veld, A. Kohlmeyer, S. G. Moore, T. D. Nguyen, R. Shan, M. J. Stevens, J. Tranchida, C. Trott, and S. J. Plimpton, *Comp. Phys. Comm.* **271**, 108171 (2022).
- [60] D. R. Heine, G. S. Grest, and E. B. Webb, *Physical Review E* **70**, [10.1103/physreve.70.011606](https://doi.org/10.1103/physreve.70.011606) (2004).
- [61] J. S. Allen, *Journal of Colloid and Interface Science* **261**, 481–489 (2003).
- [62] V. A. Lubarda and K. A. Talke, *Langmuir* **27**, 10705–10713 (2011).
- [63] M. Iwamoto, H. Ino, T. Kimura, and Y. Kishimoto, *Nano Studies* **8**, 29 (2013).
- [64] P. E. Theodorakis, E. A. Müller, R. V. Craster, and O. K. Matar, *Soft Matter* **11**, 9254 (2015).
- [65] P. Katre, B. Mahapatra, M. Karmakar, S. Jagdish, N. K. Chandra, and A. Kumar, *Proceedings of the National Academy of Sciences* **123**, [10.1073/pnas.2528750123](https://doi.org/10.1073/pnas.2528750123) (2026).